Sensitivity Analysis of Uncertainty in Model Prediction

Trent Russi,* Andrew Packard, Ryan Feeley, and Michael Frenklach*

Department of Mechanical Engineering, University of California, Berkeley, California 94720-1740

Received: August 27, 2007; In Final Form: November 28, 2007

Data Collaboration is a framework designed to make inferences from experimental observations in the context of an underlying model. In the prior studies, the methodology was applied to prediction on chemical kinetics models, consistency of a reaction system, and discrimination among competing reaction models. The present work advances Data Collaboration by developing sensitivity analysis of uncertainty in model prediction with respect to uncertainty in experimental observations and model parameters. Evaluation of sensitivity coefficients is performed alongside the solution of the general optimization ansatz of Data Collaboration. The obtained sensitivity coefficients allow one to determine which experiment/parameter uncertainty contributes the most to the uncertainty in model prediction, rank such effects, consider new or even hypothetical experiments to perform, and combine the uncertainty analysis with the cost of uncertainty reduction, thereby providing guidance in selecting an experimental/theoretical strategy for community action.

1. Introduction

Predictive ability of chemical kinetics models, as of models in general, is one of the most sought after characteristics that underlie scientific activity in reaction chemistry. Reliable model predictions are needed for both establishment of poorly understood reaction mechanisms and quantitative application of established mechanisms. The current level of predictiveness in most cases is far from satisfactory, and one is interested in identifying possible actions that could measurably improve it: What causes/skews the model predictiveness? Are there new experiments to be performed, old ones to be repeated, and/or theoretical studies to be carried out? What impact could a planned experimental work have? What would it take to bring a given chemical kinetics model to a desired level of accuracy? In the present report, we present an approach to address such questions.

The mathematical quest for the model predictiveness typically relies upon sensitivity analysis,[1−4] parameter tuning/optimization,[5−14] and propagation of errors.[14−21] The two-stage approach is common: estimation of model parameters and their uncertainties (generally, from experimental data) followed by the analysis of the influence of the estimated parameter values and uncertainties on model prediction. So doing commits to best-fit parameter values, often having individual, uncorrelated uncertainties. In an alternative approach, one transfers uncertainties in the experimental data into model prediction directly. The most common techniques for this use Bayesian methods.[20,22] The same goal can be accomplished with some loss of statistical information (e.g., the structure of distributions) but with an enormous gain in computational efficiency by a deterministic method we call Data Collaboration. The mathematical formalism of Data Collaboration is presented in refs 23−28 and briefly reported in the next section. Here, we illustrate the underlying ideas with the following pictorial example.

Consider a chemical reaction system that is described by a kinetic model with two parameters, rate constants k_1 and k_2, and is used to predict an observable Y_P, say a product concentration, Y, at conditions P. The initial information available is the range of uncertainty for each of the rate constants. This is shown in the top left panel of Figure 1, where the area colored in green designates the k_1-k_2 space corresponding to the individual k_1 and k_2 spans. In other words, the green area represents the set of (k_1, k_2) pairs that satisfy the given initial information; we refer to this set as prior knowledge and designate it by the letter H.

For every (k_1, k_2) point in H, there is a model prediction, y. For all (k_1, k_2) points in H, there is a set of predictions, which are shown in Figure 1 as the blue surface for conditions P. Also indicated in Figure 1 is the span of values predicted for Y_P, limited from below by the minimum point of the blue surface, $y_{P,min}$, and from above by the maximum one, $y_{P,max}$.

Let us now assume that we perform a new experiment, A, on the reaction system and that the observed Y_A at these conditions is inferred from measurements to be within the range ($y_{A,min}$, $y_{A,max}$). We ask this: what is the span of the model predictions for observable Y at conditions P, ($y_{P,min}$, $y_{P,max}$), given as before that k_1 and k_2 are constrained to their respective prior ranges of uncertainties, H, and now with an additional condition that the model prediction for the new experiment must be within the uncertainty of its observed value, ($y_{A,min}$, $y_{A,max}$)? This is illustrated in the top right panel of Figure 1: only part of the green area satisfies the compound condition that (k_1, k_2) is within H and the predicted Y_A is within the ($y_{A,min}$, $y_{A,max}$) range. This smaller area is colored in red and referred to as a feasible set, F. As a consequence of the smaller k_1-k_2 domain of the feasible set, as compared to the prior knowledge, the span of predicted Y_P (i.e., the range of the red surface) is decreased.

Performing another experiment, B, results in further reduction in the possible (k_1, k_2) values, that is, in a smaller feasible set. However, the smaller feasible set does not necessarily lead to the reduction in the span of predicted Y_P, as illustrated in the bottom left panel of Figure 1. Yet another experiment shrinks both the feasible set and the prediction interval, as shown in the bottom right panel of Figure 1.

* To whom correspondence should be addressed. E-mail: (T.R.) trussi@berkeley.edu; (M.F.) myf@me.berkeley.edu.

10.1021/jp076861c CCC: $40.75
Published on Web 02/28/2008

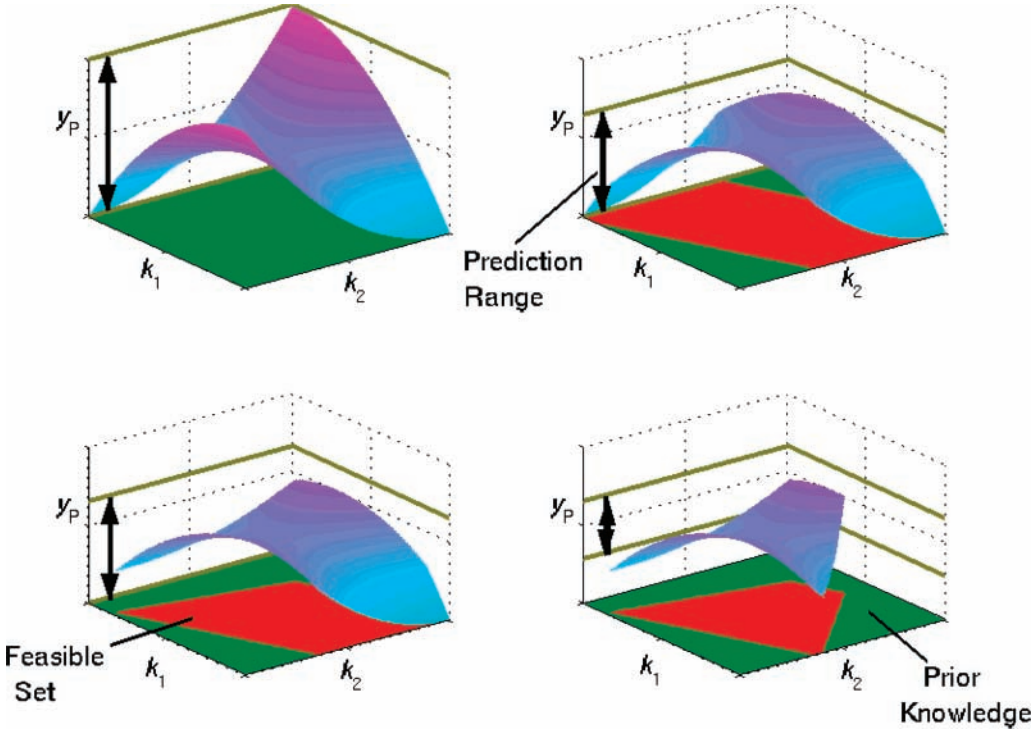

Figure 1. Illustration of model prediction on the feasible set (see text).

This example illustrates the way experimental data increase our knowledge of the system of interest: a new experiment reduces possible combinations of parameter values, thereby decreasing the range of variability (i.e., uncertainty) in a model prediction. The methodology of Data Collaboration formalizes the "transfer" of the uncertainty in a given experimental observation (or theoretical evaluation) to the uncertainty in a desired model prediction and does so by imposing all (experimental and theoretical) constraints at once. At the same time, satisfying an increasing number of constraints shrinks the parameter feasible set, which may (but often does not[24,29]) decrease the uncertainty in the parameter values as well. Typically, the geometry of the feasible set is very complex.[24,29] Data Collaboration, which fully exploits the properties of the feasible set, treats the feasible set geometry as a "derived" feature in information transfer from data to prediction.

In previous studies, we addressed the collaborative features of this approach,[24] mutual consistency of a set of experiments,[24,25] and discrimination among competing reaction models.[26] In the present study, we return to our initial objective:[23] model prediction. We show that Data Collaboration allows one to assess the propagation of uncertainty more deeply, determining which experiment/parameter uncertainty contributes the most to the current uncertainty in model prediction, ranking such effects and considering new or even hypothetical experiments, thereby providing guidance in selecting next experiments to perform.

We begin with a brief description of Data Collaboration concepts and definitions in Section 2. We then present the new mathematical developments regarding experiment and parameter uncertainty in Sections 3 and 4. Finally, we demonstrate these new developments with several examples in Section 5.

2. Data Collaboration

Data Collaboration is a framework designed to make inferences from experimental observations in the context of an underlying model.[23−26] An observable, Y, is experimentally measured and modeled using a reaction kinetics system. M is a model predicting Y, and d is the measured value. The measurement has an uncertainty bounded by l from below and by u from above, $l \leq M - d \leq u$. The triple of measurement d, uncertainty l and u, and model M for a given set of conditions is referred to as a dataset unit. A collection of dataset units, whose elements are indexed by e ranging from 1 to m, is referred to as a dataset.

Each model, M_e, has a functional dependence on a set of model parameters, active variables $\mathbf{X}_e$. Different models may have different active variable sets with some in common and some unique to each. Their union is denoted $\mathbf{X} = \cup_{e=1}^{m} \mathbf{X}_e$. The value x_i of each parameter X_i is bounded by prior knowledge, expert-assessed uncertainties of the form $x_{i,\min} \leq x_i \leq x_{i,\max}$. Collectively, all dataset parameter values, x, span the prior knowledge "hypercube" $H = \{\mathbf{x} \in \mathrm{R}^n : x_{i,\min} \leq x_i \leq x_{i,\max}\}$. The component-wise projection of x onto the active variables $\mathbf{X}_e$ is denoted $\mathbf{x}_e$. The subset of the hypercube satisfying $l_e \leq M_e(x_e) - d_e \leq u_e$ for all dataset units is referred to as the feasible set, F.

The feasible set expresses the collective constraints imposed by experiment and theory. One of the essential features of Data Collaboration is making model predictions while constraining model parameters to the feasible set. The underlying numerical methods are Solution Mapping,[1,5,30] polynomial optimization,[31] and semidefinite programming.[27,32]

3. Problem Statement

Given a dataset composed of several dataset units, we seek to quantify the influence of each dataset unit on the prediction of an unmeasured observable Y_P. We do not have the measurement, but have a model, M_P, designed to reproduce the observable. This model is dependent on a set of parameters X_P, a subset of X, and evaluating it at any point in the feasible set yields a valid model prediction.

A concise way to represent the uncertainty in this prediction is to form a prediction interval that encloses all values M_P can take over the feasible set. The length of this interval

$$R_{P,F} = \max_{\mathbf{x}\in F} M_P(\mathbf{x}_P) - \min_{\mathbf{x}\in F} M_P(\mathbf{x}_P) \quad (1)$$

is the uncertainty in predicting the unmeasured observable Y_P with the subscript F serving as a reminder of the dependence of the prediction range on the feasible set. The objective of the present study is assessing the influence of the quantified dataset uncertainty (reported uncertainties in each experiment and in each parameter of the dataset) on the length of the prediction interval. This could be done through a brute force approach by, for instance, excluding an experiment or reducing its uncertainty by half and recomputing the prediction interval. Here, we develop a methodology of assessing the influence by quantifying the local dependence of the prediction interval on the experiment and parameter uncertainties. For this purpose, we introduce sensitivity coefficients

$$\lambda_e^P \sim \frac{\partial(\text{prediction interval})}{\partial(\text{uncertainty in } d_e)},\ \nu_i^P \sim \frac{\partial(\text{prediction interval})}{\partial(\text{uncertainty in } x_i)} \quad (2)$$

that provide measures of how much the prediction interval $R_{P,F}$ changes when the uncertainty in measurement d_e or parameter x_i is perturbed. The explicit expressions for λ's and ν's are developed in Section 4. An important feature of our method is that the sensitivity coefficients are obtained while computing $R_{P,F}$. This makes it computationally feasible to evaluate λ's and ν's for many M_P's, an aspect utilized in Section 5.3.

4. Sensitivity Coefficients

4.1. Mathematical Expressions. We begin development of expressions for λ_e^P and ν_i^P by rewriting the experimental constraints $l_e \le M_e(\mathbf{x}_e) - d_e \le u_e$ as $L_e \le M_e(\mathbf{x}_e) \le U_e$, where $L_e = l_e + d_e$ and $U_e = u_e + d_e$, and expressing the length of the prediction interval introduced in eq 1 as $R_{P,F} = \bar{M}_P - \underline{M}_P$ where

$$\bar{M}_P = \max_{\mathbf{x}} M_P(\mathbf{x}_P)$$
$$\text{subject to: } \begin{cases} x_{i,\min} \le x_i \le x_{i,\max} & \text{for } i = 1, \ldots, n \\ L_e \le M_e(\mathbf{x}_e) \le U_e & \text{for } e = 1, \ldots, m \end{cases} \quad (3)$$

$$\underline{M}_P = \min_{\mathbf{x}} M_P(\mathbf{x}_P)$$
$$\text{subject to: } \begin{cases} x_{i,\min} \le x_i \le x_{i,\max} & \text{for } i = 1, \ldots, n \\ L_e \le M_e(\mathbf{x}_e) \le U_e & \text{for } e = 1, \ldots, m \end{cases} \quad (4)$$

The constrained optimization, formulated in eqs 3 and 4, is in general nonconvex and thus difficult to solve exactly. Our method for tackling such problems, described in Section 4.2, yields Lagrange multipliers that are essentially partial derivatives of the maximum $\bar{M}_P$ and minimum $\underline{M}_P$ to the constraining bounds $x_{i,\min}$, $x_{i,\max}$, L_e, and U_e. For clarity in subsequent manipulations, these are notated as

$$\bar{\mu}_{L_e} = -\frac{\partial \bar{M}_P}{\partial L_e},\quad \bar{\mu}_{U_e} = \frac{\partial \bar{M}_P}{\partial U_e},\quad \underline{\mu}_{L_e} = \frac{\partial \underline{M}_P}{\partial L_e},\quad \underline{\mu}_{U_e} = -\frac{\partial \underline{M}_P}{\partial U_e}$$
$$\bar{\mu}_{x_{i,\min}} = -\frac{\partial \bar{M}_P}{\partial x_{i,\min}},\quad \bar{\mu}_{x_{i,\max}} = \frac{\partial \bar{M}_P}{\partial x_{i,\max}},\quad \underline{\mu}_{x_{i,\min}} = \frac{\partial \underline{M}_P}{\partial x_{i,\min}},\quad \underline{\mu}_{x_{i,\max}} = -\frac{\partial \underline{M}_P}{\partial x_{i,\max}} \quad (5)$$

The sensitivity coefficients conceptually defined in eq 2 are formulated as

$$\lambda_e^P = \frac{1}{2}(\bar{\mu}_{L_e} + \bar{\mu}_{U_e} + \underline{\mu}_{L_e} + \underline{\mu}_{U_e}),$$
$$\nu_i^P = \frac{1}{2}(\bar{\mu}_{x_{i,\min}} + \bar{\mu}_{x_{i,\max}} + \underline{\mu}_{x_{i,\min}} + \underline{\mu}_{x_{i,\max}}) \quad (6)$$

We now justify these expressions, focusing on λ_e^P, the sensitivity coefficients with respect to experiment uncertainty. The sensitivity coefficients ν_i^P with respect to parameter uncertainty are derived in an analogous manner and are omitted for brevity.

Assume that a dataset experiment, for example, e, is repeated with the objective of increasing its accuracy by reducing the length of its uncertainty interval, $U_e - L_e$. We introduce $\beta \in [0, 1]$ to be the fraction reduction in the uncertainty interval. When repeating this experiment, the measured value d_e may also change, and so we define α as a shifting factor, taking values between -1 and $1 - \beta$. This range of α is chosen so that the new interval intersects the old interval at least at one point. Using these definitions, we introduce functions

$$L_{e,\alpha} = L_e + \Delta L_e$$
$$U_{e,\alpha} = U_e + \Delta U_e \quad (7)$$

where $\Delta L_e = (\alpha + \beta)(U_e - L_e)$ and $\Delta U_e = \alpha(U_e - L_e)$. As α takes on values from -1 to $1 - \beta$, the family of intervals $[L_{e,\alpha}, U_{e,\alpha}]$ parametrizes all intervals of length $(1 - \beta)(U_e - L_e)$ that intersect $[L_e, U_e]$. The following derivation considers this family of intervals, because while the measured data from the repeated experiment will fix α, it is unknown a priori.

The change in the prediction interval due to changes in L_e and U_e can now be expressed as

$$\Delta R_{P,F} = \Delta \bar{M}_P - \Delta \underline{M}_P$$
$$\overset{(a)}{\approx} (-\bar{\mu}_{L_e}\Delta L_e + \bar{\mu}_{U_e}\Delta U_e) - (\underline{\mu}_{L_e}\Delta L_e - \underline{\mu}_{U_e}\Delta U_e)$$
$$\overset{(b)}{=} [-\bar{\mu}_{L_e}(\alpha + \beta) + \bar{\mu}_{U_e}\alpha - \underline{\mu}_{L_e}(\alpha + \beta) + \underline{\mu}_{U_e}\alpha](U_e - L_e) \quad (8)$$

where (a) comes from finite difference approximations to the partial derivatives in eq 5, and (b) is from the use of the relations in eq 7. Because the remeasured value of d_e, and hence α, is unknown, we focus on the average value of $\Delta R_{P,F}$. Employing the finite difference approximation (eq 8a) and taking α to be symmetrically distributed over its range $[-1, 1 - \beta]$ results in

$$\text{average } \Delta R_{P,F} \approx -\frac{1}{2}(\bar{\mu}_{L_e} + \bar{\mu}_{U_e} + \underline{\mu}_{L_e} + \underline{\mu}_{U_e})\beta(U_e - L_e) \quad (9)$$

Noting that $-\beta(U_e - L_e) = \Delta$(uncertainty in d_e), the interpretation of λ_e^{P} as given in eq 2 results by dividing eq 9 by Δ(uncertainty in d_e) and taking the limit as Δ(uncertainty in d_e) approaches zero.

4.2. Evaluation Method. We begin this section by recapping pertinent results of optimization theory,[32] focusing on constrained optimization and sensitivity interpretation of Lagrange multipliers. We then discuss how the special case of quadratic cost function and quadratic constraint functions, those employed by the Data Collaboration, gives rise to more refined results.

Consider a constrained optimization problem

$$p^\star = \min_{\mathbf{x}\in\mathbf{R}^n} f(\mathbf{x})$$
$$\text{subject to } g_i(\mathbf{x}) \le 0 \text{ for } i = 1, \ldots, m \tag{10}$$

where a real-valued function f is minimized, subject to several inequality constraints involving the minimization variable. The dual optimization, which introduces Lagrangian multipliers, is

$$d^\star = \max_{\lambda\in\mathbf{R}^m} \min_{\mathbf{x}\in\mathbf{R}^n} f(\mathbf{x}) + \lambda^T g(\mathbf{x})$$
$$\text{subject to } \lambda_i \ge 0 \text{ for } i = 1, \ldots, m \tag{11}$$

The inequality $d^\star \le p^\star$ always holds. Moreover, if $p^\star$ is written as a function of nonzero constraint bounds, namely

$$p^\star(\mathbf{u}) = \min_{\mathbf{x}\in\mathbf{R}^n} f(\mathbf{x})$$
$$\text{subject to } g_i(\mathbf{x}) \le u_i \text{ for } i = 1, \ldots, m \tag{12}$$

and if $\lambda^\star$ is the (vector) optimizer for the Lagrangian dual problem in eq 11, the bound

$$p^\star(\mathbf{u}) \ge d^\star - \lambda^{\star T}\mathbf{u} \tag{13}$$

holds for all $\mathbf{u} \in \mathbf{R}^m$. Note that large entries of $\lambda^\star$ imply high sensitivity of the optimum value in eq 12 to constraint tightening (negative values for entries of $\mathbf{u}$), while small values imply low sensitivity to constraint loosening.

Recent results in optimization[32,33] state that if the function f and the functions g_i are quadratic functions, then the problem (eq 11) is readily solved by semidefinite programming (SDP), and the optimal $\lambda^\star$ is obtained. However, because the second-order terms of f and g_i are not necessarily positive-semidefinite, it is not the case that the original problem (eq 10) is necessarily easily solved. Therefore eq 13 is quite useful; it provides a lower bound and quantitative sensitivity information about the solution to a problem that is difficult to solve.

In application of Data Collaboration to nonlinear dynamic models, the dataset-unit models M are approximated by quadratic surrogate functions of active variables,[24,25,27] and hence the prediction optimizations are converted to quadratic optimizations. As discussed above, the optimal Lagrange multiplier $\lambda^\star$ is obtained reliably and efficiently using SDP. The partial derivatives used in eq 5 are approximated by the components of $\lambda^\star$. As eq 13 holds for all u, the entries of $\lambda^\star$ may be considered to be "global sensitivities".

5. Results and Discussion

This section presents several example uses of the sensitivity coefficients introduced in eq 2. We begin by calculating these coefficients for a specific case, discuss implications of the computed values, and delineate the difference from the traditional sensitivity analysis. Then, we introduce a means to gauge the general impact of an experiment in a dataset by averaging the sensitivity coefficients determined for multiple model predictions. We conclude with the formulation and solution of two related resource allocation problems that might guide further experimentation by accounting for the cost associated with reducing experiment/parameter uncertainty.

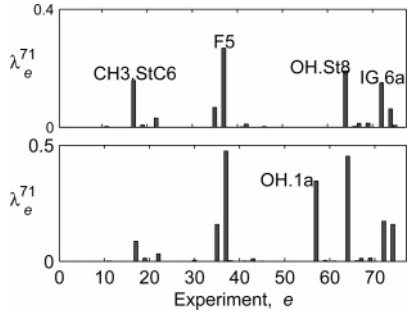

Figure 2. Sensitivity coefficients of the prediction interval $R_{71,F}$ with respect to the uncertainties of the remaining 76 dataset experiments. The top panel uses an uncertainty of 0.1 for all experiments; the ranking of the top sensitivities is: $e = 37, 64, 17, 72, 35, 74, 22$. The bottom panel uses different sensitivities (see Section 5.2); the ranking of the top sensitivities is: $e = 37, 64, 57, 72, 74, 34, 17, 22$.

We illustrate the methodology with the dataset used in our prior studies,[24−26] namely the GRI-Mech 3.0 dataset.[34] This is a collection of models and experimental results used to study chemical kinetic models of pollutant formation in combustion of natural gas. The GRI-Mech 3.0 dataset consists of 77 dataset units (experimental targets) and a 102-dimensional parameter vector. The model in each dataset unit is a quadratic surrogate, expressing $\log_{10}$ of the experimental target in terms of $\log_{10}$ of parameters (typically pre-exponential factors of the Arrhenius expressions), normalized to take values between -1 and $+1$.

Due to insufficient records of experiment uncertainties even for such a well-documented case as GRI-Mech 3.0, an artificial yet realistic assignment $L_e = d_e - 0.1$ and $U_e = d_e + 0.1$ was used for "nominal" uncertainties of all dataset units, $e = 1, \ldots, 77$. As the uncertainty level of each dataset unit can influence the analysis, at the suggestion of an anonymous reviewer we extended the example using nonconstant experimental uncertainties. The parameter uncertainties $[x_{i,\min}, x_{i,\max}]$, for $i = 1, \ldots, 102$, were taken as reported.[34] The results of Sections 5.1, 5.3, and 5.4 were obtained using the 0.1 uncertainty level, while Section 5.2 considers nonconstant levels.

5.1. Direct Evaluation of Sensitivity Coefficients. As a concrete example, we considered the observable of the GRI-Mech 3.0 dataset unit 71, Y_{71}, the laminar flame speed in a stoichiometric atmospheric ethane-air mixture[35] (target StF8 of GRI-Mech 3.0[34]). We ignored the measured flame speed 40.2 cm/s of this observable and removed its unit from the dataset. Taking M_{P} to be M_{71} in eq 1, the Data Collaboration analysis predicted the interval [34.5, 58.4] cm/s based on the dataset comprised of the remaining 76 units. The length of the prediction interval in this case is $R_{71,F} = \bar{M}_{71} - \underline{M}_{71} = \log_{10} 58.4 - \log_{10} 34.5$. The analysis also yielded the sensitivity coefficients λ_e^{71} for each of the experiments $e = 1, \ldots, 70, 72, \ldots, 77$ and ν_i^{71} for each parameter i in the dataset, which are displayed in the top panel of Figures 2 and 3, respectively.

Inspection of the top panel of Figure 2 reveals that the largest sensitivity value corresponds to dataset unit 37, laminar flame speed of a stoichiometric methane−air mixture at an elevated pressure of 4.9 atm,[36] target F5 of GRI-Mech 3.0.[34] The computed value of the sensitivity coefficient is $\nu_{37}^{71} = 0.27$,

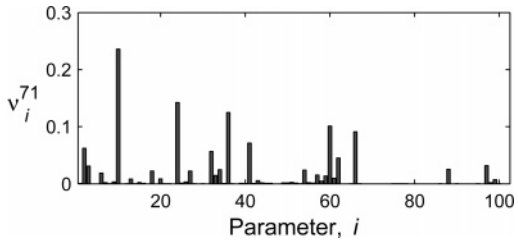

Figure 3. Sensitivity coefficients of the prediction interval $R_{71,F}$ with respect to the uncertainties in the model parameters; the ranking of the top sensitivities is: i = 10, 24, 36, 60, 66, 41, 2, 32, 62, 97, 3, 88, 34, 54.

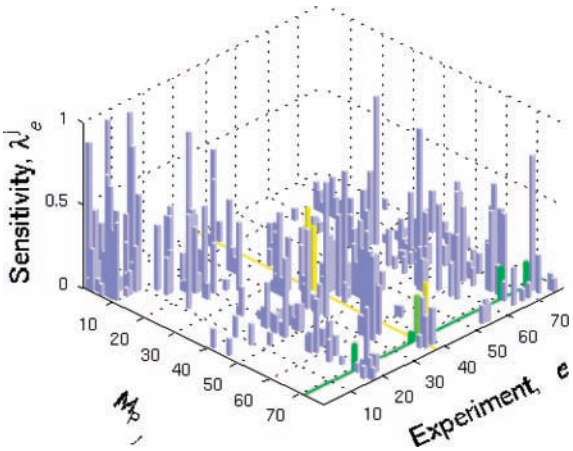

Figure 4. Sensitivity coefficients of the predicted interval with respect to the experiment uncertainties performed for each of the dataset units. Each GRI-Mech 3.0 model, M_{P_j}, is predicted in turn using the remaining GRI-Mech 3.0 dataset units. Sensitivities computed for the uncertainty in predicting Y_{71} with respect to the uncertainties of the remaining GRI-Mech 3.0 dataset observables are highlighted green. Sensitivities for the uncertainty in predicting each GRI-Mech 3.0 observable to uncertainty in experiment 37 are highlighted yellow.

which projects, from 0.27 $\approx \Delta(\bar{M}_{71} - \underline{M}_{71})/\Delta(U_{37} - L_{37})$, a reduction by 11.7 and 21.1% in the predicted range in the flame speed if the uncertainty interval $\Delta(U_{37} - L_{37})$ is reduced by factors of 2 and 10, respectively. Computations performed with such reduced ranges for $\Delta(U_{37} - L_{37})$ resulted in corresponding intervals [36.8, 58.4] and [39.2, 58.4] cm/s, that is, a reduction by 12.5 and 24.4% in the predicted range of the flame speed, close to the respective estimates 11.7 and 21.1%.

The sensitivity spectrum in the top panel of Figure 2 exhibits the effect sparsity[37,38]—the predicted range is affected significantly by the uncertainties of only a small number of experiments in the dataset, and most have negligible impact on the prediction. It is noteworthy, as exemplified by the top panel of Figure 2, that the prediction interval for one type of experiment, a flame speed, is measurably influenced by the uncertainty of different experimental systems, in this case shock-tube species peaks (e = 64, 17; GRI-Mech 3.0 targets OH.ST8 and CH3.StC6, respectively), shock-tube ignition (e = 72; target IG.6a), and flame speed at different conditions (e = 35, 74; targets F3 and F1).

The results presented for Y_{71}, sensitivity to various types of experiments and effect sparsity, are not atypical. The calculations can be repeated for different choices of M_P. Figure 4 displays the results of 77 such individual Data Collaboration computations, performed by designating in turn each of the dataset units to be the unperformed experiment for which we seek the range of model prediction based on the rest of the dataset information. The green row in this figure marks the sensitivities depicted in the top panel of Figure 2. The bars in each row parallel to the green row rank experiments whose uncertainty impacts the prediction interval for the particular observable. The bars in the perpendicular direction rank experiments mostly affected by the uncertainty of a given experiment.

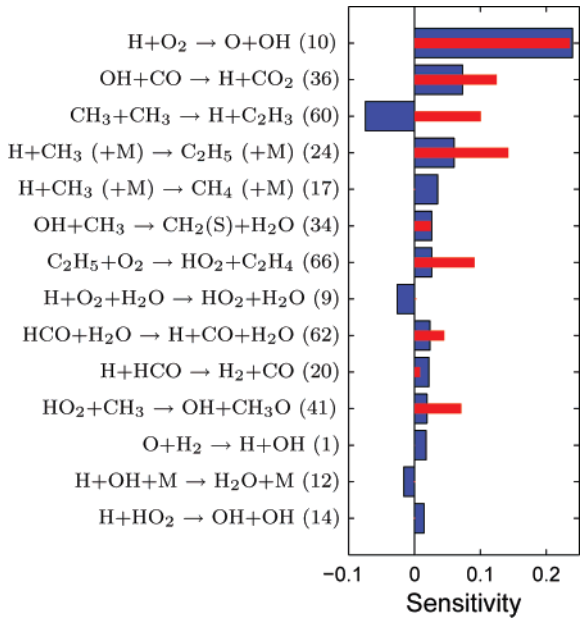

Figure 5. Logarithmic response sensitivity of laminar flame speed in a stoichiometric atmospheric ethane-air mixture, Y_{71}, with respect to reaction rate coefficients, k, $\partial \ln y_{71}/\partial \ln k_i$ (blue bars), sorted in decreasing order.[34] The corresponding ν_i^{71} is shown as red bars. The numbers in parentheses refer to the index i of the corresponding model parameter.

The sensitivity information, such as that illustrated in the top panel of Figure 2 and in Figure 4, have important practical applications. If one desires to improve the quality of the model prediction (for an unknown property), the sensitivity spectrum identifies possible experiments in the dataset to be remeasured with a tighter control of the respective experiment uncertainties. If the desired range of the model prediction is specified, one can perform Data Collaboration computations for a series of "what if" scenarios with varying individual experiment uncertainties, exploring the feasibility of attaining the stated goal and establishing a possible experimental strategy. The same numerical procedures can be used to explore the impact of performing an additional experiment at a different condition or with a different apparatus. We will continue this discussion in Section 5.4.

It is important to emphasize that the results just discussed demonstrate Data Collaboration's ability to propagate uncertainty from experimental observations to model prediction, subject to prior knowledge of parameter bounds, in a single step. Next, we demonstrate that by using Data Collaboration we can assess the impact of parameter bounds as well, and that this information is not exactly the same as obtained in the usual sensitivity analysis.

Figure 3 displays sensitivity coefficients ν_i^{71} for the same response of e = 71 as in the top panel of Figure 2 but with respect to the parameter ranges. These sensitivity coefficients gauge the dependence of the prediction interval, $R_{P,F}$, on variation in a parameter uncertainty, while the usual sensitivity coefficients measure the dependence of the predicted value, M_P, on the variation in a parameter value. The two sets of sensitivities are overlaid in Figure 5. While there are similarities, there are also significant differences between the two sets.

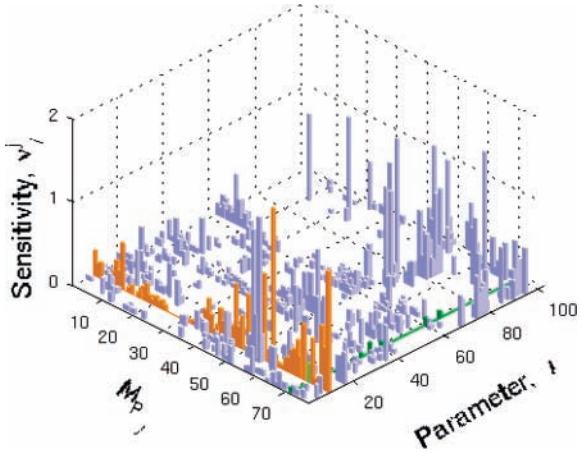

Figure 6. Sensitivity coefficients of the predicted interval with respect to parameter uncertainties performed for each of the dataset units. Each GRI-Mech 3.0 model, M_{P_j}, is predicted in turn using the rest of the GRI-Mech 3.0 dataset. Sensitivities computed for the uncertainty in predicting Y_{71} with respect to the uncertainties in the 102 model parameters are highlighted in green. The sensitivities for each GRI-Mech 3.0 observable to uncertainty in parameter 10 are highlighted orange.

The "by-value" sensitivities can be either negative or positive; increasing some rate coefficients increases the predicted flame speed while increasing others decreases it. On the other hand, the "by-uncertainty" sensitivities, which are those introduced in the present work, are only positive; increasing uncertainty of a parameter can only increase the predicted interval (the same is true for the sensitivities with respect to experiment uncertainty, those displayed in the top panel of Figure 2 and in Figure 4).

Another interesting observation follows from comparison of the sensitivity rankings seen in Figure 5. In both measures, parameter $i = 10$ is ranked highest. However the two sensitivity measures generally rank other parameters differently. For example, parameter $i = 24$ is ranked fourth with by-value sensitivity but second in the by-uncertainty ranking. Similarly third-ranked by-uncertainty ($i = 36$) is second-ranked by-value. Comparing rankings for $i = 17$ and $i = 24$ shows further differences worth noting. The by-value sensitivity indicates that M_P (M_{71} in this case) has modest sensitivity to both of these parameters (fourth and fifth ranked, respectively). By contrast, the by-uncertainty sensitivity coefficients are very different, namely 0 for $i = 17$ (i.e., bottom ranked) yet second-ranked for $i = 24$.

When the optimization in eqs 3 and 4 is constrained only by parameter ranges, $x_{i,\min} \le x_i \le x_{i,\max}$, the resulting by-uncertainty sensitivity values and spectra overall are close to the by-value ones (exactly equal for a linear M_P). This result reveals the nature of the difference between the two sensitivity measures. The by-uncertainty sensitivity "incorporates" additional information, originating from experiment uncertainty constraints.

Figure 6 is similar to Figure 4, except that it displays the sensitivity coefficients ν_i^P with respect to parameter uncertainties for the same 77 Data Collaboration computations. The green row in Figure 6 indicates the sensitivities depicted in Figure 3. For each row parallel to the green row, the bars rank parameters whose uncertainty impacts the prediction interval for the particular observable. The bars in the perpendicular direction rank observables whose predictions are most affected by the uncertainty of a given parameter.

The sensitivity information, such as that illustrated in Figures 3 and 6, can be used analogously to the discussed above sensitivity spectra with respect to experiment uncertainty:

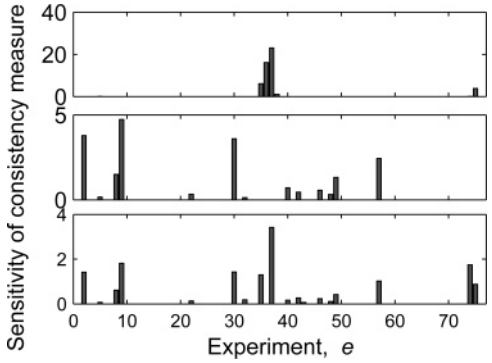

Figure 7. Sensitivity coefficients of dataset consistency measure with respect to experiment uncertainty. The top panel displays sensitivities when time measurements have uncertainty 0.05, flame speeds 0.02, temperatures 0.01, and all other experiments 0.1 (inconsistent dataset). The middle panel has flame speed uncertainties increased to 0.05 (inconsistent dataset). The bottom panel has time measurement uncertainties increased to 0.08 (consistent dataset).

identification of parameters for uncertainty reduction and performance of "what if" analysis for such reductions. Perhaps the primary source for reduction of uncertainty in an individual parameter has become the use of theory, for example, applying high-level quantum-chemical methods. Data Collaboration unifies experiment and theory; both influence the "extraction" of knowledge by reducing the respective uncertainty bounds and the results of both are used in unison, as mathematically equivalent constraints in a single optimization problem. Further unification is attained by assigning cost to uncertainty reduction, as discussed in Section 5.4.

5.2. Sensitivity Analysis with Uneven Uncertainties. In the previous example, an uncertainty of 0.1 for each experiment in the GRI-Mech 3.0 dataset was used. In general, one would expect each experiment to have its own uncertainty. We now extend the previous example by giving the experiments differing uncertainties that are hypothetical, yet not without basis: those in reaction-progress times were set to 0.05, flame speeds to 0.02, temperatures to 0.01, and the rest were kept at 0.1, as before. This essentially created a new dataset with the same observations, d_e, but different uncertainties, u_e.

Making this assignment of uncertainties resulted in the dataset being inconsistent, meaning there did not exist a parameter vector that satisfied all the constraints.[24,25] To examine the source of the inconsistency, the sensitivities of the consistency measure (as defined in eq 2 in ref 25) to the uncertainty in the experiments were computed using the techniques of Data Collaboration.[25] The highest sensitivities corresponded to the flame speed measurement uncertainties (see top panel of Figure 7). Hence, the uncertainty in the flame speed experiments was increased to 0.05. Recomputing the consistency measure revealed that the time measurements had the highest sensitivity coefficients (middle panel of Figure 7). The time measurement uncertainties were then set to 0.08, which made the dataset consistent (resulting in the sensitivities in the bottom panel of Figure 7).

An interval prediction on unit 71 was performed using the dataset created in the above manner. The experiment sensitivity coefficients with respect to uncertainty are shown in the bottom panel of Figure 2. They have the same order of magnitude as those in the top panel of Figure 2 and exhibit most of the same peaks. One noticeable difference is the sensitivity to the uncertainty in experiment 57 (a time measurement in a shock tube experiment, target OH.1a of the GRI-Mech 3.0 dataset[34]), which appears using the newly assigned uncertainty levels and

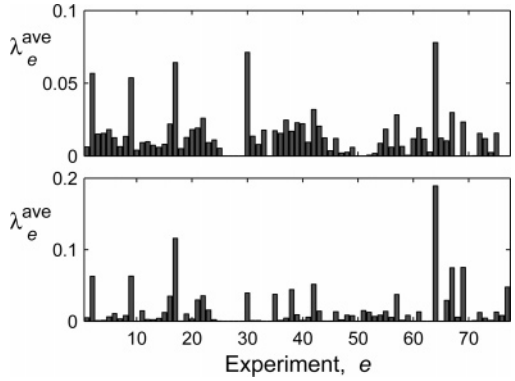

Figure 8. Average sensitivity coefficients of the prediction interval with respect to experiment uncertainties. Top panel, averaged over 77 dataset units; bottom panel, averaged over 10 000 random models.

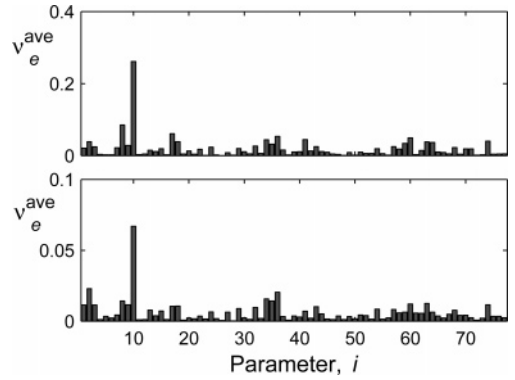

Figure 9. Average sensitivity coefficients of the prediction interval with respect to parameter uncertainties. Top panel, averaged over 77 dataset units; bottom panel, averaged over 10 000 random models.

is negligibly small when using the 0.1 uncertainties. It is clear that each set of uncertainties leads to a specific outcome.

5.3. Averaging Sensitivity Coefficients to Assess Experiment Impact. The quantity λ_e^{P} assesses the influence of uncertainty in experiment e on the uncertainty in predicting a specific observable. Can a general measure of the influence of the eth experiment uncertainty be developed? One approach to obtaining such a measure is to average $\lambda_e^{\mathrm{P}_j}$, $j = 1, \ldots, p$, from predictions for a diverse set of p observables. We denote this average by λ_e^{ave}. Similarly, ν_i^{ave} measures the average influence of uncertainty in parameter x_i. Determination of these average measures requires assembling a diverse set of observables and constructing their models. In this section we describe two different approaches to accomplish these. Both produce close results, thereby cross-validating each other.

The first approach to obtain a set of diverse observables is simply to use those already present in the dataset. Thus, we obtained λ_e^{ave} and ν_i^{ave} by averaging over the given set of dataset units. These values are displayed in the top panel of Figures 8 and 9.

Another avenue to obtaining and modeling a collection of diverse observables is to generate a set of *random models*, $\{M_{\mathrm{P}j}\}_{j=1}^{p}$, that are similar to the dataset models, $\{M_e\}_{e=1}^{m}$. This diverse set provides a much larger set to average prediction sensitivities over to obtain a more general measure of experiment impact. Each GRI-Mech dataset-unit model is a quadratic function, $M_e(\mathbf{x}_e) = \mathbf{x}_e^{\mathrm{T}}\mathbf{A}_e\mathbf{x}_e + \mathbf{b}_e\mathbf{x}_e + c_e$, where $\mathbf{A}_e$, $\mathbf{b}_e$, and c_e are fitted coefficients. A random model, M_{P_j}, is formulated to have the same structure. Active variables, $\mathbf{X}_{\mathrm{P}_j}$, of the random models are selected by ensuring that every pair of variables appearing in a random model appears together as active variables in at least one of the models of the GRI-Mech 3.0 dataset. Coefficients $\mathbf{A}_{\mathrm{P}_j}$ and $\mathbf{b}_{\mathrm{P}_j}$ are obtained by sampling a standard normal distribution and then scaled so that

$$||\mathbf{A}_{\mathrm{P}_j}||_F = \frac{1}{77}\sum_{e=1}^{77}||\mathbf{A}_e||_F, \qquad \text{and } ||\mathbf{b}_{\mathrm{P}_j}||_F = \frac{1}{77}\sum_{e=1}^{77}||\mathbf{b}_e||_F \quad (14)$$

where $||\ ||_F$ denotes the matrix norm. Equation 14 constrains the coefficients of the quadratic form of a random model to be of similar magnitudes as those of the dataset models and also preserves the relative magnitude of the quadratic terms $\mathbf{A}_{\mathrm{P}_j}$ as compared to the linear terms $\mathbf{b}_{\mathrm{P}_j}$. The constant term c_{P_j} was set to zero because it does not affect the sensitivities λ_e^{ave} and ν_i^{ave}.

Ten thousand random models were generated in this manner, and the sensitivity coefficients $\{\lambda_e^{\mathrm{P}_j}\}_{e=1}^{77}$ and $\{\nu_i^{\mathrm{P}_j}\}_{i=1}^{102}$ were computed for each random model, $j = 1, \ldots, 10\,000$. These values were averaged over the 10 000 random models to obtain λ_e^{ave} and ν_i^{ave}, which are displayed in the bottom panels of Figures 8 and 9, respectively. Comparison between the two sets of results in Figures 8 and 9, the respective random and over-dataset averages, indicates a general accord in the ranking. This level of agreement is encouraging for the use of the random model approach. For example, the sensitivity of prediction range to the uncertainty in experiment 64 is high both when averaged over predictions of the GRI-Mech 3.0 observables and when averaged over predictions of the observables of random models generated by eq 14. On this basis, we conclude that the present level of uncertainty in experiment 64 is likely to affect prediction of combustion observables within the class of condition covered by GRI-Mech 3.0. Consequently, such predictions may benefit from lowering the uncertainty in experiment 64. Analysis of future actions may take into account additional considerations and is discussed next.

5.4. Cost-Constrained Uncertainty Quantification. In Sections 5.1 and 5.3, the Data Collaboration methodology was used to obtain sensitivities that rank impact of uncertainties in experiments and/or parameters on model prediction. Such sensitivity spectra allow one to identify highest-ranking experiments and/or parameters, gain insights on possible future actions to undertake for improving model predictability, and test the developed ideas in "what if" computational scenarios. In considering different scenarios, one introduces additional factors of a practical nature. For instance, it could be easier to remeasure the second-ranked target with a twofold increased accuracy than to reduce the uncertainty of the highest-ranked one by 10%. Alternatively, it could be easier to use a high-level theory on some top-ranked parameters than to perform new measurements. The methodology of Data Collaboration allows one to formalize such assessments and by doing so to unify on the fundamental level experiment and theory. We illustrate the approach with the following example.

We introduce cost functions K_e and K_i associated with reduction in uncertainty intervals of experimental observations and parameters, respectively. From practical considerations, one knows that higher accuracy in both measurements and numerical calculations requires more resources, and this dependence is unlikely to take a linear mathematical form. Also, the cost functions representing this dependence should produce a cost of zero for no uncertainty reduction and attribute a very large (or infinite cost) to reducing the uncertainty to zero. Given such cost functions, we pose the following question:

Given a budget T, determine the best experimental/theoretical strategy for reducing the uncertainty of model prediction for the given response, $R_{\mathrm{P},F}$.

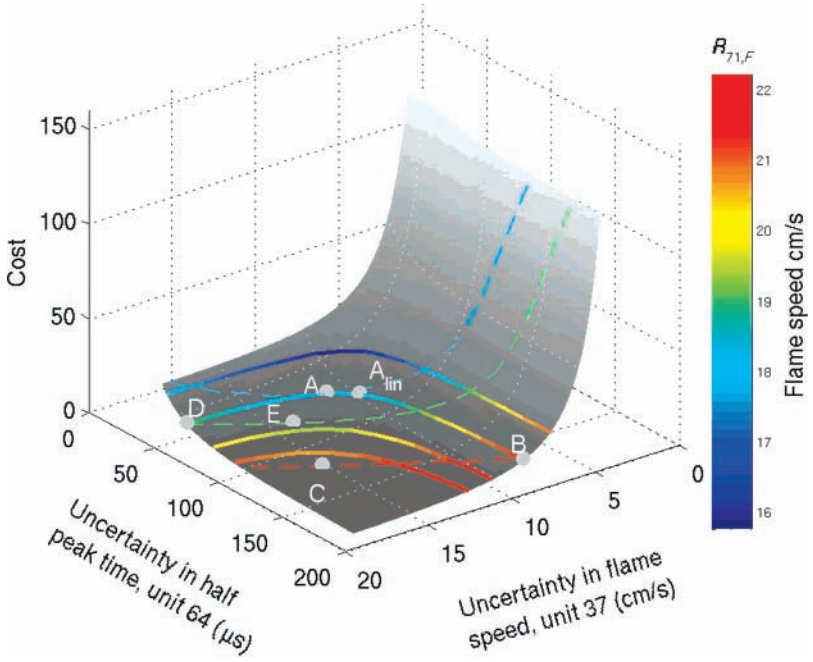

Figure 10. Cost of reduction in uncertainty of dataset units 37 and 64. The solid horizontal lines are constant-budget lines drawn at $T = 3$, 5, 10, 20; they color code the value of the prediction interval computed for dataset unit 71, $R_{71,F}$, according to the color bar displayed on the right of the figure. The dashed lines are drawn at constant values of $R_{71,F}$, 17.5, 19.1, and 21.3. The coordinates (μs, cm/s) of the marked points are A (68.8, 11.0), B (185.8, 8.3), C (117.9, 15.2), D (56.0, 18.4), E (83.7, 13.1), and A_{lin} (78.6, 9.8). The total-cost values, T, at points C and E are 2.2 and 5.7, respectively.

To address this allocation problem, we denote the current uncertainty in the measurement of Y_e as $\delta_{e,\mathrm{cur}} = U_e - L_e$ (the subscript "cur" meaning current), and the cost of remeasuring Y_e with a smaller measurement uncertainty, δ_e, as $K_e(\delta_e)$. Similarly, $\delta_{i,\mathrm{cur}} = x_{i,\max} - x_{i,\min}$ is the current uncertainty in parameter x_i, and $K_i(\delta_i)$ is the cost of reducing the uncertainty in parameter i from $\delta_{i,\mathrm{cur}}$ to δ_i. In the following, we denote by the boldface $\boldsymbol{\delta}$ the combined vector of the uncertainties, containing δ_e for $e = 1, \ldots, m$ and δ_i for $i = 1, \ldots, n$.

Recasting eq 1 such that experiment and parameter uncertainties are allowed to vary, we express $R_{\mathrm{P},F}$ as a function of $\boldsymbol{\delta}$:

$$R_{\mathrm{P},F}(\boldsymbol{\delta}) = \max_{\mathbf{x}} M_{\mathrm{P}}(\mathbf{x}_{\mathrm{P}}) - \min_{\mathbf{x}} M_{\mathrm{P}}(\mathbf{x}_{\mathrm{P}})$$
$$\text{subject to: } \begin{cases} L_e + 0.5(\delta_{e,\mathrm{cur}} - \delta_e) \le M_e(\mathbf{x}_e) \le U_e - 0.5(\delta_{e,\mathrm{cur}} - \delta_e) \\ x_{i,\min} + 0.5(\delta_{i,\mathrm{cur}} - \delta_i) \le x_i \le x_{i,\max} - 0.5(\delta_{i,\mathrm{cur}} - \delta_i) \end{cases}$$
$$\text{for each } e = 1, \ldots, m \text{ and } i = 1, \ldots, n \tag{15}$$

The formulation in eq 15 presumes that for each uncertainty interval the lower and upper bounds are drawn together equally. An assumption of this type is necessary because the solution to the posed question depends on the updated uncertainty intervals themselves, which are unknown a priori. With this in mind, the resource allocation problem is

$$\boldsymbol{\delta}^{\mathrm{opt}} = \underset{\boldsymbol{\delta}}{\operatorname{argmin}} \; (R_{\mathrm{P},F}(\boldsymbol{\delta}))$$
$$\text{subject to: } \begin{cases} \sum_{e=1}^{m} K_e(\delta_e) + \sum_{i=1}^{n} K_i(\delta_i) \le T \\ 0 \le \delta_e \le \delta_{e,\mathrm{cur}} \\ 0 \le \delta_i \le \delta_{i,\mathrm{cur}} \end{cases} \tag{16}$$
$$\text{for each } e = 1, \ldots, m \; i = 1, \ldots, n$$

As a concrete example, we will use, as before, $M_{\mathrm{P}} = M_{71}$ for model prediction with the 76 remaining GRI-Mech 3.0 units as the given dataset. To present the solution graphically, we limit the analysis to two variables. From the sensitivity spectrum given in Figure 2, we select the top two dataset units, 37 and 64, as candidates for uncertainty reduction. The observable of dataset unit 37 is laminar flame speed of a stoichiometric methane−air mixture at a pressure of 4.9 atm,[36] target F5 of GRI-Mech 3.0[34] and that of unit 64 is half time to the OH concentration peak in observed in a shock-tube oxidation of methane,[39] target OH.ST8.

To each of the selected observables, we assign a cost function that meters the uncertainty reduction. A plausible functional form, which possesses the properties described above, is

$$K(\delta) = \left(\frac{\delta_{\mathrm{cur}}}{\delta}\right)^{a} - 1 \tag{17}$$

Taking the parameter $a > 0$, the functional form of eq 17 represents a nonlinear rise in cost with the reduction in uncertainty, and the steepness of the rise is metered by the value of a. With no reduction, $\delta = \delta_{\mathrm{cur}}$ and the cost is zero. Complete elimination of uncertainty, $\delta = 0$, results in an infinitely large cost. For the present example, the values of parameter a in eq 17 are chosen arbitrarily as $a_{37} = 3$ and $a_{64} = 2$.

Having selected two experiments to be performed again and having specified the cost functions, we then solved the example problem: Given a budget T, determine the best experimental strategy for reducing the uncertainty of the model prediction for Y_{71}, the laminar flame speed in a stoichiometric atmospheric ethane−air mixture. The optimization in eq 16 is difficult to solve in general because the function that maps experiment and parameter uncertainties onto model prediction (eq 15) is complicated. For the present example, with two free variables, we employed a "brute-force" method, by gridding the uncertainty space, solving the prediction in eq 15 at each grid node, and interpolating to find prediction interval lengths along constant-budget lines. The number of grid points, g, was set to 40 per dimension, resulting in 1600 computations of $R_{\mathrm{P},F}(\boldsymbol{\delta})$.

The numerical results are presented in Figure 10. The gray surface represents a total cost of decreasing the uncertainties in the flame and shock-tube measurements. The upper front corner of this surface marks the assigned, "current uncertainties" in the respective two measurements. The solid horizontal lines are constant-budget lines, drawn at $T = 3, 5, 10, 20$; they are colored according to the value of the prediction interval, $R_{71,F}$, whose color-scale is displayed on the right of the figure. The dashed lines are drawn at constant values of $R_{71,F}$.

Inspection of the color coding of the constant-budget lines indicates that for a budget of $T = 10$ the lowest prediction range, 17.5 cm/s, marked as point A, is obtained by decreasing uncertainties of both experiments by about one-half each. If only one of the experiments, for example 37, is to be repeated with the same budget of 10, the prediction range, marked as point B, is much larger at 21.3 cm/s. Following the dashed line from point B shows that the same prediction-interval value could be obtained at a much lower cost, $T = 2.2$ (Point C), if both experiments are repeated. Analogous results and conclusions arise if experiment 64 is repeated alone.

The gridding and interpolation method we employed in our example scales exponentially with the number of experiments, m, and parameters, n, as the function in eq 16 is evaluated g^{n+m} times. With two free variables, the computational time to obtain the data depicted in Figure 10 was 7 h. In the special case when a local search algorithm works, it can take substantially less time. For example, a local search algorithm starting at δ_{cur} explored much less of the space and took 20 min to find Point A.

A dramatic reduction in computational cost can be achieved using the results of the present study. We linearize eq 16 and observe that the outcome utilizes our sensitivity coefficients

$$R_{\text{P},F}(\delta) \approx R_{\text{P},F}(\delta_{\text{cur}}) + \sum_{e=1}^{m} \lambda_e^{\text{P}}(\delta_e - \delta_{e,\text{cur}}) + \sum_{i=1}^{n} \nu_i^{\text{P}}(\delta_i - \delta_{i,\text{cur}}) \quad (18)$$

If the cost functions K_e and K_i in eq 16 are convex, then the problem (the constraints of eq 16 and the objective from eq 18) has a linear objective, box constraints, and a constraint that is the sum of convex functions, each depending on a different scalar variable. The time to solve this new problem scales favorably, $\sim(n + m)^{\sigma}$, where σ is a relatively small, positive number.[32] The requirement on K_e and K_i of convexity is satisfied by the nature of the cost's dependence on decreasing uncertainty.

Applying the linearized solution to our earlier example, again only allowing δ_{37} and δ_{64} to vary and using a budget of $T = 10$, found Point A_{lin} and corresponding $R_{\text{P},F} = 17.8$ cm/s (Figure 9). This is within 2% of the Point A solution of 17.5 cm/s and took less than 0.1 s to compute (on a 2.8 GHz Pentium 4 desktop PC). With such computational efficiency, it is affordable to solve a larger problem. For instance, allowing all variables to vary (the remaining 76 GRI-Mech 3.0 experiment uncertainties and all 102 parameter uncertainties), the optimization took 30 s. In that test, all cost functions were given the same exponent, $a = 2$. Solving this optimization suggested reduction of uncertainty in 5 experiments ($e = 37, 64, 17, 72$, in that order) and 10 parameters ($i = 24, 41, 60, 66, 32, 10, 34, 62, 36, 2$).

A related question can be similarly stated: Given a desired value of the prediction interval for a given Y_{P}, $R_{\text{P},F}^{\max}$, determine experimental/theoretical strategy to attain this objective with the lowest cost. We write this problem as the optimization

$$\delta^{\text{opt}} = \underset{\delta}{\operatorname{argmin}} \sum_{e=1}^{m} K_e(\delta_e) + \sum_{i=1}^{n} K_i(\delta_i) \quad \text{subject to: } \begin{cases} R_{\text{P},F}(\delta) \le R_{\text{P},F}^{\max} \\ 0 \le \delta_e \le \delta_{e,\text{cur}} \\ 0 \le \delta_i \le \delta_{i,\text{cur}} \end{cases} \quad \text{for each } e = 1, \ldots, m \; i = 1, \ldots, n \quad (19)$$

This optimization is solved in a manner analogous to the previous one.

6. Summary

The analysis introduced in this work offers a methodology of applying the infrastructure of Data Collaboration to obtain sensitivities that rank impact of uncertainties in experiments and/or parameters on uncertainty in model prediction. Such sensitivity spectra allows one to identify highest-ranking experiments and/or parameters, provide insights on possible future actions to undertake for improving model predictability, and test the developed ideas in "what if" computational scenarios. By focusing on reliability of model prediction and considering practical costs of possible actions, the methodology exploits experiment, theory, models, and communal data with a unified analysis that can help to identify the optimal course of community action.

Acknowledgment. The work was supported by the NSF Chemistry Division, Cyber-enabled Chemistry, Grant CHE-0535542.

References and Notes

(1) Miller, D.; Frenklach, M. *Int. J. Chem. Kinet.* **1983**, *15*, 677−696.
(2) Zádor, J.; Zsély, I. G.; Turányi, T.; Ratto, M.; Tarantola, S.; Saltelli, A. *J. Phys. Chem. A* **2005**, *109*, 9795−9807.
(3) Brown, N. J.; Revzan, K. L. *Int. J. Chem. Kinet.* **2005**, *37*, 538−553.
(4) Scire, J. J. J.; Dryer, F. L.; Yetter, R. A. *Int. J. Chem. Kinet.* **2001**, *33*, 784−802.
(5) Frenklach, M. Modeling. In *Combustion Chemistry*; Gardiner, W. C., Jr., Ed.; Springer-Verlag: New York, 1984.
(6) Frenklach, M.; Wang, H.; Rabinowitz, M. J. *Prog. Energy Combust. Sci.* **1992**, *18*, 47−73.
(7) He, F.; Marshall, A. G. *J. Phys. Chem. A* **2000**, *104*, 562−567.
(8) Donahue, N. M.; Clarke, J. S. *Int. J. Chem. Kinet.* **2004**, *36*, 259−272.
(9) Tang, W.; Zhang, L.; Linninger, A. A.; Tranter, R. S.; Brezinsky, K. *Ind. Eng. Chem. Res.* **2005**, *44*, 3626−3637.
(10) Singer, A. B.; Taylor, J. W.; Barton, P. I.; Green, W. H. *J. Phys. Chem. A* **2006**, *110*, 971−976.
(11) Elbern, H.; Schmidt, H.; Talagrand, O.; Ebel, A. *Environ. Modell. Software* **2000**, *15*, 539−548.
(12) Sandu, A.; Liao, W.; Carmichael, G.; Henze, D.; Seinfeld, J. *Aerosol Sci. Tech.* **2005**, *39*, 677−694.
(13) Mendoza-Dominguez, A.; Russell, A. *Environ. Sci. Technol.* **2000**, *34*, 4974−4981.
(14) Wang, L.; Milford, J.; Carter, W. *Atmos. Environ.* **2000**, *34*, 4337−4348.
(15) Tellinghuisen, J. *J. Phys. Chem. A* **2001**, *105*, 3917−3921.
(16) Phenix, B. D.; Dinaro, J. L.; Tatang, M. A.; Tester, J. W.; Howard, J. B.; McRae, G. J. *Combust. Flame* **1998**, *112*, 132−146.
(17) Brown, M. J.; Smith, D. B.; Taylor, S. C. *Combust. Flame* **1999**, *117*, 652−656.
(18) Reagan, M. T.; Najm, H. N.; Pébay, P. P.; Knio, O. M.; Ghanem, R. G. *Int. J. Chem. Kinet.* **2005**, *37*, 368-382.
(19) Wang, L.; Milford, J.; Carter, W. *Atmos. Environ.* **2002**, *36*, 115−135.
(20) Bergin, M.; Milford, J. *Atmos. Environ.* **2000**, *34*, 781-792.
(21) Gao, D.; Stockwell, W.; Milford, J. *J. Geophys. Res.* **1996**, *101*, 9107−9119.

(22) Bayarri, M.; Berger, J.; Paulo, R.; Sacks, J.; Cafeo, J.; Cavendish, J.; Lin, C.; Tu, J. *Technometrics* **2007**, *49*, 138−154.
(23) Frenklach, M.; Packard, A.; Seiler, P. In *Proceedings of the American Control Conference*; IEEE: New York, 2002.
(24) Frenklach, M.; Packard, A.; Seiler, P.; Feeley, R. *Int. J. Chem. Kinet.* **2004**, *36*, 57−66.
(25) Feeley, R.; Seiler, P.; Packard, A.; Frenklach, M. *J. Phys. Chem. A* **2004**, *108*, 9573−9583.
(26) Feeley, R.; Frenklach, M.; Onsum, M.; Russi, T.; Arkin, A.; Packard, A. *J. Phys. Chem. A* **2006**, *110*, 6803−6813.
(27) Seiler, P.; Frenklach, M.; Packard, A.; Feeley, R. *Optim. Eng.* **2006**, *7*, 459−478.
(28) Frenklach, M. *Proc. Combust. Inst.* **2007**, *31*, 125−140.
(29) Gutenkunst, R. N.; Waterfall, J. J.; Casey, F. P.; Brown, K. S.; Myers, C. R.; Sethna, J. P. *PLoS Comput. Biol.* **2007**, 3.
(30) Frenklach, M.; Packard, A.; Feeley, R. Optimization of reaction models with Solution Mapping. In *Comprehensive Chemical Kinetics*, Vol. 42; Carr, R. W., Ed.; Elsevier: New York, in press.
(31) Parrilo, P. *Math. Program., Ser. B* **2003**, *96*, 293−320.
(32) Boyd, S.; Vandenberghe, L. *Convex Optimization*; Cambridge University Press: Cambridge, UK, 2004.
(33) Sturm, J. *Opt. Methods Software* **1999**, *11*−*12*, 625−653. Available at http://sedumi.mcmaster.ca/.
(34) Smith, G. P.; Golden, D. M.; Frenklach, M.; Moriarty, N. W.; Eiteneer, B.; Goldenberg, M.; Bowman, C. T.; Hanson, R. K.; Song, S.; Gardiner, W. C., Jr.; Lissianski, V. V.; Qin, Z. GRI-Mech 3.0. http://www.me.berkeley.edu/gri_mech/ (last accessed February 2008).
(35) Vagelopoulos, C. M.; Egolfopoulos, F. N. *Proc. Combust. Inst.* **1998**, *27*, 513−519.
(36) Just, T. Private communication, 1994.
(37) Box, G. E. P.; Meyer, R. D. *J. Res. Nat. Bur. Stand.* **1987**, *90*, 494−500.
(38) Myers, R. H.; Montgomery, D. C. *Response Surface Methodology*; Wiley: New York, 2002.
(39) Yu, C. L.; Wang., C.; Frenklach, M. *J. Phys. Chem.* **1995**, *99*, 14377−14387.